High-Temperature Kinetics of the Reaction between Chlorine Atoms and Hydrogen Sulfide

Yide Gao, I. M. Alecu, A. Goumri, and Paul Marshall*

Department of Chemistry, University of North Texas, 1155 Union Circle #305070, Denton, Texas 76203-5070, USA

* To whom correspondence should be addressed.

E-mail: marshall@unt.edu Tel (940) 565-2294

Abstract

The rate constant k_1 for Cl + H_2S has been measured over 290-914 K using the laser flash photolysis/resonance fluorescence technique. Atomic chlorine was generated by pulsed 193 nm photolysis of CCl_4 and C_6H_5Cl and monitored by time-resolved resonance fluorescence at 130-140 nm. The data are summarized as $k_1 = (2.90 \pm 0.10) \times 10^{-11} \exp(2.38 \pm 0.11 \text{ kJ mol}^{-1}/RT)$ cm^3 molecule^{-1} s^{-1} where the uncertainties in the Arrhenius parameters are $\pm 2\sigma$. 95% confidence limits for k_1 are ±6%. These extended range measurements confirm a negative activation energy for the reaction.

1. Introduction

The reaction

$$Cl + H_2S \rightarrow SH + HCl \quad (1)$$

is of dynamic interest as a protypical heavy-light-heavy system of atoms [1]. Several studies have focused on the production of vibrationally excited products whose distribution may readily be monitored by infra-red techniques, and a population inversion between newly formed HCl(v=0) and HCl(v=1) allows laser action [2]. Reaction 1 may also be of significance in the atmosphere of Venus, where it could couple sulfur and chlorine chemistry, and possibly in the terrestrial atmosphere (such as volcanic plumes) and combustion systems as well.

Dill and Heydtmann generated Cl atoms in a discharge through Cl_2 at low pressures and detected infrared chemiluminescence (IRCL) from HCl in v>0 [3]. Leone and co-workers used laser flash photolysis (LFP) of precursor molecules to generate atomic chlorine, and monitored the IRCL of the HCl product, attributed mainly to HCl in the v=1 and v=2 states [4, 5]. Agrawalla and Setser were able to detect the weak emission from vibrationally excited SD produced via

$$Cl + D_2S \rightarrow SD + DCl \quad (2)$$

and deduced that approximately 3% of the reaction exoergicity led to SD vibrational excitation, with 7±4% of the SD produced in v=1 [6]. Hossenlopp et al. monitored the DCl distribution via time-resolved IR diode laser spectroscopy, and found the ratio for v=0:v=1:v=2 to be 0.33:0.56:0.11 [7]. The most recent dynamics study by Chen et al. was based on time-resolved FTIR monitoring of reaction 1, and these workers obtained the ratio for v=0:v=1:v=2 to be 0.41:0.52:0.07 [8]. These distributions are consistent with the general interpretation of heavy-

light-heavy systems, where most of the energy release is expected to result in excitation of the new H-Cl bond [1].

There is uncertainty about the detailed mechanism of reaction 1. One possibility is direct abstraction, but an addition/elimination pathway has been discussed by several groups [5, 9, 10]. The *ab initio* work of Wilson and Hirst indicated the existence of a bound H_2S-Cl adduct, but not whether it could decompose to SH + HCl [11]. They also characterized a transition state (TS) for direct abstraction. Their transition state theory calculations for direct abstraction gave a room temperature rate constant an order of magnitude below that observed, which left open the possibility that addition/elimination dominates the kinetics. Resende et al. explored this possibility but obtained a rate constant about 15 times larger than experiment at room temperature [12]. Nicovich et al. commented that the available dynamics data "do not appear to allow clear differentiation between the two possible mechanisms" [10]. Subsequently, Chen et al. were unable to explain their measured rotational energy distributions in terms of a direct abstraction model, and speculated that an addition/elimination model might rationalize their observations [8].

Prior measurements of the rate constant k_1 for reaction 1 are listed in Table 1. It may be seen that at room temperature these span a factor of 3. In addition to some of the IR studies mentioned already, kinetic data have been obtained via the discharge-flow (DF) method combined with resonance fluorescence (RF) and molecular-beam mass spectrometry (MBMS) detection [13, 14], via flashlamp photolysis (FP) or LFP combined with RF detection [9, 10], and via relative rate (RR) measurements where radioactive ^{38}Cl was produced by irradiation of CF_3Cl [15]. As well as disagreements concerning the magnitude of k_1, there are disagreements concerning its temperature dependence, where zero or slightly negative activation energies (E_a)

have been reported [9, 10, 15]. The NASA-JPL critical evaluation [16] is based on the kinetics studies of Nicovich et al. [10], who applied the LFP-RF technique over 200-430 K to both reactions 1 and 2.

The main aim of the present work is to extend the temperature range for k_1, to more closely determine its temperature dependence. Incidentally, our extension to beyond 900 K encompasses all high-temperature regions of the Venusian atmosphere including down to the surface.

2. Apparatus and Methodology

2.1. Gas Preparation and Handling

Hydrogen sulfide (purity 99.5% Matheson Gas Products) and tetrachloromethane (purity $\geq$ 99.9%, Spectrum) were purified via several freeze-pump-thaw cycles and then mixed with a large excess of Argon (purity 99.9999%, Air Liquide) to a pressure of roughly 1300 mbar in Pyrex bulbs. Flows of the gas mixtures were combined after passage through mass flow controllers (MKS Instruments Types 1159A and 1159B), which were calibrated against a Teledyne Hastings-Raydist bubble meter (HBM-1A). Typical flow rates were up to about 0.3 μmol s^{-1} for H_2S, about 3 μmol s^{-1} for CCl_4, and (70 - 700) μmol s^{-1} for Ar. Pressures were measured with a capacitance manometer (MKS Instruments Type 622A).

2.2. Reactor and Detection System

The reactor is a three-way stainless steel cross, as shown in Figure 1. The intersection region establishes a reaction zone of roughly 8 cm^3. The six side arms are each 11 cm long, as measured from the reaction zone boundaries, with an inner diameter of 2.2 cm. Nichrome

resistance heating wire, electrically insulated with ceramic beads, is wrapped along the inner 7 cm portion of each side arm. The reactor is housed in thermal insulation, 20 cm on a side, made of 2.5 cm thick alumina boards (Zircar Products ZAL-50). The outermost 1.5 cm portions of each side arm extend past the insulation, and are water-cooled. Connections are made through standard ISO NW25 KF fittings.

Pulsed radiation from the laser enters the reactor at right angles to the continuous probe resonance radiation, and fluorescence is detected through a mutually perpendicular side arm. Two of the side arms are used for conducting the gas mixtures in and out of the reactor while another serves as a port for a thermocouple. The sheathed Type K thermocouple (chromel/alumel) is used to monitor the gas temperature inside the reaction zone, which is displayed on an Omega DP 285 readout. This thermocouple is not shielded against radiative heat exchange with the walls of the reactor, which can introduce radiation errors [17]. Separate experiments to derive empirical corrections have been outlined previously [18], and an uncertainty of ±2 % for the corrected temperature was recommended. The thermocouple is removed from the reaction zone during kinetic measurements. A second sheathed thermocouple is placed outside the reactor for temperature control (Omega CN 3910 KC/S).

The resonance radiation is produced from a flow of about 0.3 mbar of a dilution of 0.1% of Cl_2 in Ar through a microwave discharge flow lamp operated at powers of 30-50 W. The intensity of the fluorescence is monitored by a solar-blind UV PMT (Hamamatsu R212) operated at 2490 V (Bertran Model 215 power supply). As can be seen from Figure 1, the PMT is connected to a computer-controlled multichannel scaler (EG&G Ortec ACE) via a preamplifier/discriminator (MIT Model F-100T) to count emitted photons as a function of time. Signals following 50-5,000 laser pulses are accumulated and analyzed on a computer. The timing

of the experiments is controlled by a digital delay/pulse generator (Stanford Research Systems, DG 535), which triggers the excimer laser (MPB PSX-100, beam cross section 7 x 8 mm^2) ahead of the multichannel scaler to allow measurement of the steady background signal that arises from scattered light from the resonance lamp.

As previously mentioned, the reagents are diluted in a large excess of argon, which thermalizes the radicals generated, increases the heat capacity of the gas mixture to maintain isothermal conditions during the reactions, and slows diffusion of the transient radicals to the reactor surfaces. The average time spent by the gases in the reaction zone is long compared to the time scale of the reaction (~1 ms), so that the reactor is kinetically equivalent to a static system.

2.3. Measurements of Cl + H_2S kinetics.

Chlorine atoms were generated from CCl_4 via pulsed laser photolysis at 193 nm. This photochemistry has been studied at room temperature by Hanf et al. [19], who found a total quantum yield of 1.5 for Cl atom formation, with 27% in the $(3p)^2P_{1/2}$ excited state. At thermal equilibrium at 290 and 915 K, the fraction of ground-state $Cl(^2P_{3/2})$ is 99 and 89 %, respectively. $Cl(^2P_{1/2})$ can be quenched by collisions with Ar and CCl_4. Based on the concentrations ([Ar] ~10^{18} atoms cm^{-3} and [CCl_4] ~10^{15} molecules cm^{-3}) and quenching rate constants of 3.0×10^{-16} and 2.1×10^{-10} cm^3 $molecule^{-1}$ s^{-1} [20, 21], respectively, it may be seen that the dominant quencher is CCl_4. The collisional lifetime for excess $Cl(^2P_{1/2})$ is ~ 5 μs which is two orders of magnitude shorter than the time scale for kinetic measurements. This assures that an equilibrium population of $Cl(^2P_{3/2})$ and $Cl(^2P_{1/2})$ was studied. Calcium fluoride optics were used in order to block any H-atom radiation at 121.6 nm that might be excited by trace impurities in the resonance lamp, and no signal was observed from the photolysis of H_2S by itself.

The Cl atoms produced were allowed to react with a large excess of H_2S under pseudo-first order conditions. The rate law is given by

$$d[Cl]/dt = -k_1[Cl][H_2S] - k'[Cl] = -k_{ps1}[Cl] \quad (3)$$

where k_{ps1} is the pseudo-first-order decay coefficient. The constant k' accounts for the diffusional loss of Cl atoms, and any reaction with photolysis fragments of H_2S or CCl_4, and was seen to be effectively first order. It appears as the intercept in a linear plot of k_{ps1} vs. $[H_2S]$, the slope of which gives the corresponding second-order rate constant k_1, as shown in Figure 2.

The fluorescence intensity from Cl is proportional to its concentration, thus k_{ps1} is obtained from fitting to the signal as a function of time t. The total signal intensity I_f including the steady background B can be expressed as

$$I_f = A \exp(-k_{ps1}\, t) + B \quad (4)$$

where A and B are both constants. An example of a typical decay of fluorescence intensity signal I_f can be seen in the inset of Figure 2.

A non-linear least squares fitting algorithm [22, 23] was used to calculate k_{ps1} and its uncertainty, while the accuracy limits for the concentration of H_2S were assessed from propagation of the uncertainties in the relevant pressures and flows. The absorption cross-section and Cl quantum yield of CCl_4 ($(8.6 \pm 0.5) \times 10^{-19}$ cm^2 and 1.5 ± 0.1, respectively) [19], the photolysis beam cross section, the photolysis energy F, and $[CCl_4]$ were used to assess the initial concentration of chlorine atoms $[Cl]_0$. For this estimate of $[Cl]_0$, F was corrected by a measured factor of 0.84 to account for losses at the entry window. The value of $[Cl]_0$ is unnecessary in terms of a first-order kinetic analysis, however, knowing it enables substantiation of the pseudo first-order condition $[H_2S] >> [Cl]_0$. In a few experiments we employed an alternative photolytic precursor, C_6H_5Cl, whose use we discussed previously [24]. Typically, five $[H_2S]$ were

employed at each set of conditions, from zero to $[H_2S]_{max}$. The line through the data in Figure 2 represents a weighted linear least squares fit [25], which yields the statistical uncertainty in the slope. This uncertainty is combined with the uncertainties in temperature and H_2S/Ar dilution ratio, both of which are systematic in the course of a single determination of k_1, to yield the overall 1σ uncertainty in the second order rate constant k_1.

Chlorine atoms were monitored by time-resolved resonance fluorescence at 130-140 nm which encompasses the electronic transitions, $(4s)^2P_{3/2,1/2} \rightarrow (3p)^2P_{3/2,1/2}$ [26]. The detection sensitivity at 290 K, defined as [Cl] whose fluorescence intensity equals the standard deviation of the constant background signal, was found to be $\sim 6 \times 10^{10}$ atoms cm^{-3}. Experimental parameters such as the photolysis energy F, the pressure p, and the average gas residence time inside the reactor before photolysis, τ_{res}, were varied in order to check for any dependence of the second-order rate constants upon these parameters.

3. Results and Discussion

One hundred and six measurements over the range 289-915 K are summarized in Table 1S in the Supplementary Data section. Systematic variation of p, F, τ_{res}, and $[Cl]_0$ yielded k_1 values that were not significantly different within $\pm \sigma_{k1}$, and the independence of the rate constant from these parameters suggests that the reaction is effectively bimolecular and unaffected significantly by secondary chemistry, thermal decomposition, and mixing time. Further, changing the Cl-atom precursor at the highest and lowest temperatures did not change the observed k_1 which suggests the absence of complications involving precursor chemistry. Above 915 K the constant background signal became high, which could be indicative of heterogeneous CCl_4 dissociation. In general, the minimum non-zero $[H_2S]$ used was roughly one

quarter of $[H_2S]_{max}$, and the range of the ratio of $[H_2S]$ to $[Cl]_0$ was 6 to 116 at room temperature, with an average value of ~60.

A potential complication is the photolysis of H_2S at 193 nm to yield H + SH. H atoms do not react quickly with SH, while the rate constant for SH + Cl is 1.1×10^{-10} cm^3 $molecule^{-1}$ s^{-1} [14]. Typically photolysis laser pulses with energies of F = 0.2 – 1 mJ were employed (see the Supplementary Data). Using a photolysis cross section of 6.3×10^{-18} cm^2 $molecule^{-1}$ [16], we estimate that up to 1% of the H_2S is dissociated. This will cause a ca. 1% overestimation of k_1, which is too small to be significant and is consistent with the lack of observed dependence of k_1 on F.

As noted in the Introduction, an H_2S-Cl adduct has been predicted theoretically [11]. However, doubling the bath gas pressure at room temperature did not lead to larger k_1 values (see Table 1S). This invariance is also seen at 483 and 536 K. The data of Nicovich et al. further show there was no change in k_1 when the pressure was varied widely at room temperature [10]. The observed decays were single exponentials at all temperatures, consistent with the absence of significant adduct formation. We also comment that the computed H_2S-Cl bond dissociation enthalpy of 32 kJ mol^{-1} at 298 K [11] is too small for the adduct to be a final sink for Cl atoms above room temperature.

Table 2 shows the weighted mean k_1 values at each average temperature. The temperature dependence of the second-order rate constant is depicted in Arrhenius form in Figure 3. A linear least squares algorithm [25] was used to perform a weighted fit of ln k_1 vs 1/T based on the 1σ uncertainties in the k_1 values listed in Table 2, combined with the uncertainty in T. It yielded

$$k_1 = (2.90 \pm 0.10) \times 10^{-11} \exp(2.38 \pm 0.11 \text{ kJ mol}^{-1}/RT) \text{ cm}^3 \text{ molecule}^{-1} \text{ s}^{-1}$$

where the uncertainties in the Arrhenius parameters are ± 2σ. Combining these uncertainties with the covariance yields statistical 2σ confidence limits of 2 to 4 % for k_1 over the temperature range explored, with a minimum at the central temperature. Combination in quadrature with a 5% allowance for potential systematic errors yields final 95% confidence limits of ± 6% for k_1. Based on the above considerations, a value of $(7.6 \pm 0.5) \times 10^{-11}$ cm^3 $molecule^{-1}$ s^{-1} is obtained for k_1 at 298 K. Table 1 and Figure 4 summarize literature data for reaction 1 which have been reviewed recently [16]. There is good accord between the present results and those of Nesbitt and Leone [5] and Nicovich et al. [10], and we confirm the negative activation energy observed by the latter group. The two combined data sets can be described well by the non-Arrhenius expression $k_1 = 1.91 \times 10^{-10}$ $(T/K)^{-0.26}$ $\exp(+158\ K/T)$ cm^3 $molecule^{-1}$ s^{-1}.

As noted in the Introduction, there is not yet a quantitative understanding of the detailed mechanism for the reaction. The modestly negative activation energy, -2.4 kJ mol^{-1}, is reminiscent of that observed for alkyl radical + HBr reactions, which have been rationalized in terms of formation of an initial adduct with no energy barrier, followed by dissociation to final products over a tighter but lower energy barrier, in competition with redissociation back to the original reactants [27, 28]. Such a mechanism appears plausible here, given the published potential energy profiles [11, 12], and a theoretical analysis of reaction 1 is underway in our group.

Conclusions

The upper limit for kinetic measurements on the Cl + H_2S reaction has been extended to beyond 900 K. The data reveal a modest but clearly negative activation energy for this process.

This information may help to resolve competing models to explain the magnitude and behavior of the rate constant.

Acknowledgments

This work was supported by the Robert A. Welch Foundation (Grant B-1174).

Appendix A. Supplementary data

Supplementary data associated with this article can be found, in the online version, at http://dx.doi.org/xxxxxxxxxxxx

Table 1: Comparison of kinetic data for Cl + H_2S.

Experimental technique	k_1(298 ± 2 K) / 10^{-11} cm^3 $molecule^{-1}$ s^{-1}	$E_a \pm 2\sigma$ / kJ mol^{-1}	T range / K
LFP-IRCL[a]	6.0 ± 1.2		
LFP-IRCL[b]	7.3 ± 0.9		
DF-RF[c]	4.0 ± 0.2		
DF-MBMS[d]	5.1 ± 1.4		
FP-RF[e]	6.3 ± 0.9	0[f]	211-353
RR[g]	10.5 ± 0.4	0[f]	232-359
LFP-RF[h]	7.4 ± 1.1	-1.73 ± 0.20	202-430
LFP-FTIR[i]	3.7 ± 1.5		
LFP-RF[j]	7.6 ± 0.5	-2.38 ± 0.11	290-914

[a] ref. 4; [b] ref. 5; [c] ref. 13; [d] ref. 14; [e] ref. 9; [f] no uncertainty reported; [g] ref. 15; [h] ref. 10; [i] ref. 8; [j] current work.

Table 2: Weighted mean k_1 values for Cl + H_2S.

T / K	$k_1 \pm \sigma_{k1}$ / 10^{-11} cm^3 $molecule^{-1}$ s^{-1}
290	7.74 ± 0.09
355	6.32 ± 0.23
433	5.69 ± 0.11
483	5.34 ± 0.11
536	4.77 ± 0.19
610	4.71 ± 0.10
698	4.34 ± 0.04
815	4.14 ± 0.07
914	3.95 ± 0.05

References

[1] J.C. Polanyi, Acc. Chem. Res. 5 (1972) 161.

[2] A.T. Coombe, A.T. Pritt Jr, D. Philipovich, Chem. Phys. Lett. 35 (1975) 345.

[3] B. Dill, H. Heydtmann, Chem. Phys. 35 (1978) 161.

[4] M. Braithwaite, S.R. Leone, J. Chem. Phys. 69 (1978) 839.

[5] D.J. Nesbitt, S.R. Leone, J. Chem. Phys. 72 (1980) 1722.

[6] B.S. Agrawalla, D.W. Setser, J. Phys. Chem. 90 (1986) 2450.

[7] J.M. Hossenlopp, J.F. Hershberger, G.W. Flynn, J. Phys. Chem. 94 (1990) 1346.

[8] K.-S. Chen, S.-S. Cheng, Y.-P. Lee, J. Chem. Phys. 119 (2003) 4229.

[9] D.F. Nava, W.D. Brobst, L.J. Stief, J. Phys. Chem. 89 (1985) 4703.

[10] J.M. Nicovich, S. Wang, P.H. Wine, Int. J. Chem. Kinet. 27 (1995) 359.

[11] C. Wilson, D.M. Hirst, J. Chem. Soc. Faraday Trans. 93 (1997) 2831.

[12] S.M. Resende, J.R. Pliego, Jr., S. Vandresen, Mol. Phys. 106 (2008) 841.

[13] M.A.A. Clyne, Y. Ono, Chem. Phys. Lett. 94 (1983) 597.

[14] M.A.A. Clyne, A.J. MacRobert, T.P. Murrells, L.J. Stief, J. Chem. Soc. Faraday Trans. 2 80 (1984) 877.

[15] E.C.C. Lu, R.S. Iyer, F.S. Rowland, J. Phys. Chem. 89 (1986) 1988.

[16] S.P. Sander, R.R. Friedl, J.P.D. Abbatt, J.R. Barker, J.B. Burkholder, D.M. Golden, C.E. Kolb, M.J. Kurylo, G.K. Moortgat, P.H. Wine, R.E. Huie, V.L. Orkin, Chemical Kinetics and Photochemical data for Use in Stratospheric Modeling. Evaluation Number 17. JPL Publication 10-6 (http://jpldataeval.jpl.nasa.gov), JPL, Pasadena, 2011.

[17] A. Fontijn, W. Felder, Reactive Intermediates in the Gas Phase, Academic, New York, 1979, ch. 2.

[18] L. Ding, P. Marshall, J. Chem. Soc. Trans. 89 (1993) 419.

[19] A. Hanf, A. Lauter, H.-R. Volpp, Chem. Phys. Lett. 368 (2003) 445.

[20] G.S. Tyndall, J.J. Orlando, J. Chem. Soc. Faraday Trans. 91 (1995) 3055.

[21] R.H. Clark, D. Husain, J. Photochem. 21 (1983) 93.

[22] P. Marshall, Comput. Chem. 11 (1987) 219.

[23] P. Marshall, Comput. Chem. 13 (1989) 103.

[24] Y. Gao, P. Marshall, Chem. Phys. Lett. 469 (2009) 266.

[25] J.A. Irvin, T.I. Quickenden, J. Chem. Educ. 60 (1983) 711.

[26] H. Okabe, Photochemistry of Small Molecules, Wiley, New York, 1978.

[27] L.N. Krasnoperov, J. Peng, P. Marshall, J. Phys. Chem. A 110 (2006) 3110.

[28] D.M. Golden, J. Peng, A. Goumri, J. Yuan, P. Marshall, J. Phys. Chem. A 116 (2012) 5847.

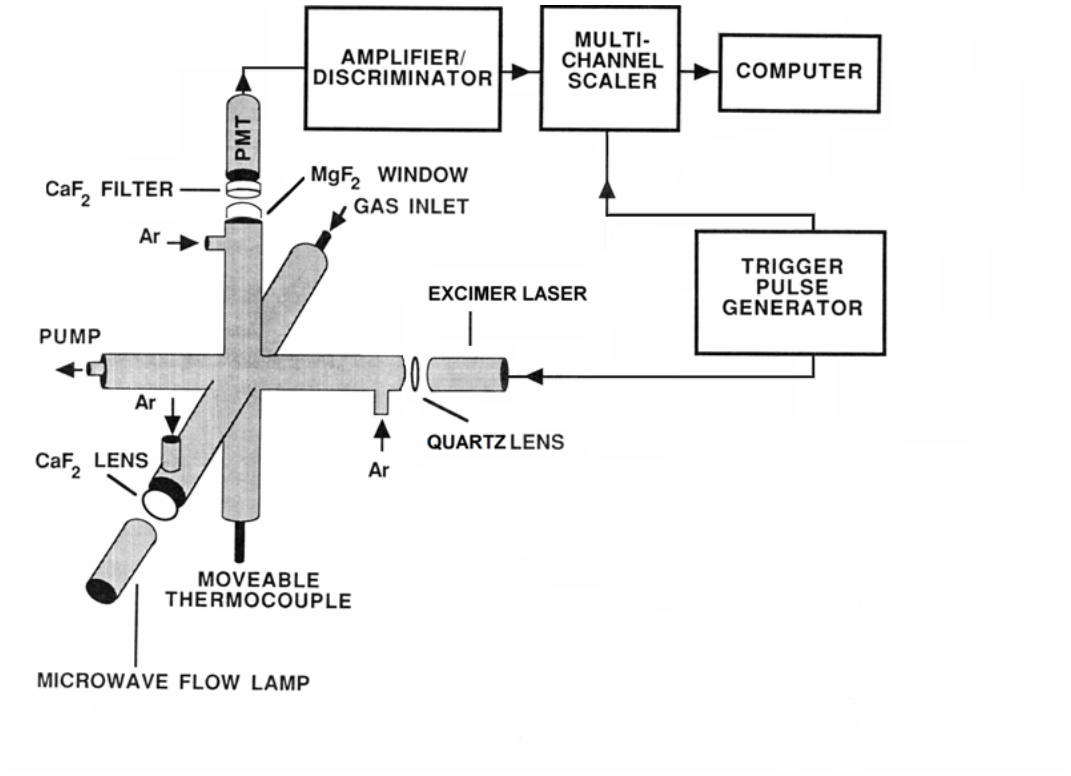

Figure 1. Schematic diagram of the apparatus used for Laser Flash Photolysis / Resonance Fluorescence measurements.

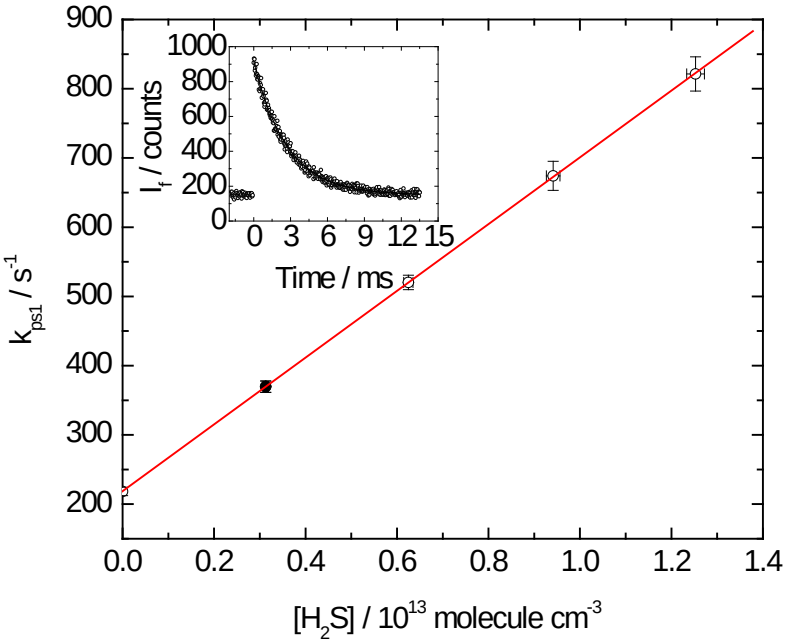

Figure 2. Plot of k_{ps1} vs [H_2S] obtained at 536 K and 21 mbar. The error bars are 2σ. The inset shows the decay of fluorescence signal plus background corresponding to the filled point.

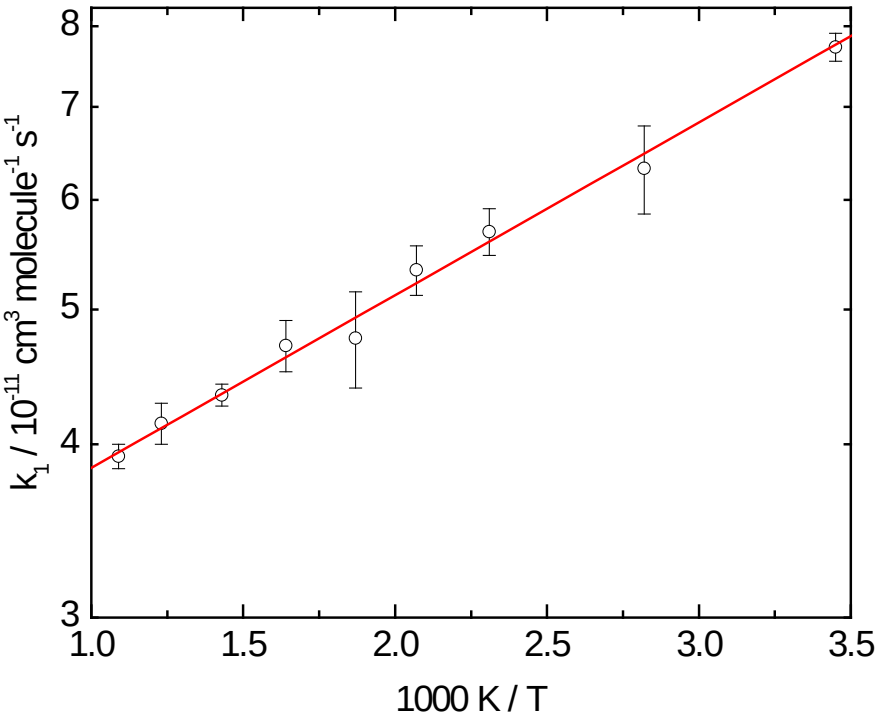

Figure 3. Arrhenius plot for Cl + H_2S. Each point represents the weighted average of the measurements at that temperature. Errors bars represent ± 2σ.

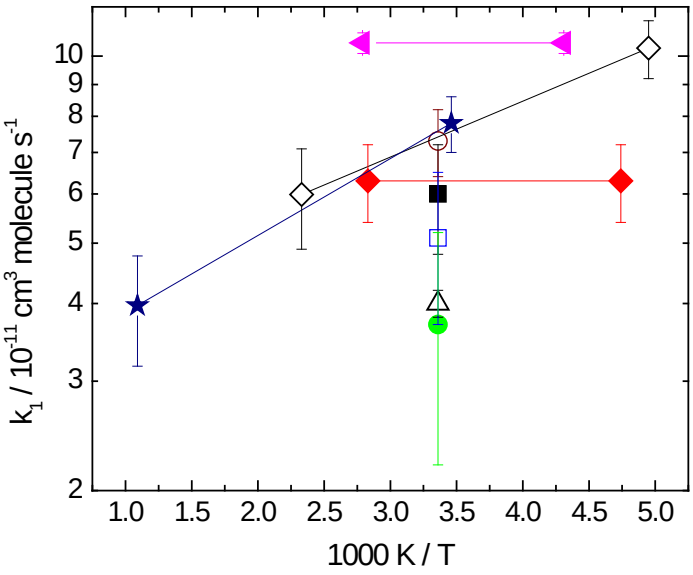

Figure. 4 Arrhenius plot of kinetic data for Cl + H_2S: filled square ref. 4; open circle ref. 5; open triangle ref. 13; open square ref. 14; filled diamond ref. 9; filled triangle ref. 15; open diamond ref. 10; filled circle ref. 8; star current work.